Desalination and Water Treatment
www.deswater.com

doi: 10.5004/dwt.2019.23470

140 (2019) 245–252
February

Study on adsorption of rhodamine B on graphene oxide/Y-type zeolite composites

Zhi-lin Cheng*, Yan-xiang Li, Zan Liu

School of Chemistry and Chemical Engineering, Yangzhou University, Yangzhou 225002, China, Tel. +86 0514 87975590; emails: zlcheng224@126.com (Z.-l. Cheng), 44059448@qq.com (Y.-x. Li), 15136851@qq.com (Z. Liu)

Received 7 May 2018; Accepted 16 November 2018

ABSTRACT

The fabrication of graphene oxide/Y-type zeolite (GY) composites with the hierarchical-porous structure was achieved by grafting GO nanosheets onto the surface of Y-type zeolite. A series of characterizations were adopted to determine the structure and properties of the GY composites. The adsorption performance of GY composites for rhodamine B (RB) in aqueous solution was examined. The effect of adsorption time, pH, adsorption temperature and initial RB concentration to adsorption capacity were intensively investigated. The adsorption behavior of the GY composites was fitting to Langmuir isotherm equation and the maximum adsorption capacity on the GY composites were up to 39.64 mg/g.

Keywords: Adsorption; Characterization; GO; Y-type; Zeolites; RB

1. Introduction

In recent years, 10%–15% of different dyes are discharged to the nature, which is a significant health hazard to environment and human even at extremely low concentrations. Among these dyes, Rhodamine B (RB) is a typical industrial dye, which is a water-soluble organic dye widely used in textile industries. The finding showed that RB could cause eye burn, irritation to skin, gastrointestinal tract, the respiratory tract and so forth. Hence, it is imperative to remove RB from the effluents before discharging back to nature.

There were many treatment techniques to get rid of these dyes from water. Among these methods, adsorption technique is deemed to be of low cost and high efficiency for removing dyes, heavy metals and other hazardous impurities from aqueous solutions [1–3]. Zeolites, as a typical porous material, have already been applied in many fields due to their high thermal stability, strong cation-exchange capacity and larger surface area. As one of industry zeolites, Y-type zeolites have a 3D channel system formed by 12-MR windows (0.76 nm in diameter), which possess the larger surface area, massive pore channel and higher pore volume [4,5]. Sannino et al. [6] reported the adsorption of agrochemical simazine onto Y-type zeolite, and intensively investigated effect of pH value, time, initial simazine concentration and solid/liquid ratio to adsorption performance. Sui et al. [7] employed the Y-type zeolite/MCM-41 composites for the adsorption of benzene and thiophene.

To the best of our knowledge, graphene oxide (GO) with few layer nanosheets had a strong propensity to interact with positively charged species such as metal ions and dyes. Tan et al. [8] found that the maximum adsorption capacity of GO for Cs (I) removing from water was up to 32.53 mg/g. Li et al. [9] reported that the adsorption capacity of graphene oxide for methylene blue attained 243.9 mg/g. Therefore, the adsorption capacity of graphene oxide for dyes or metal ions was much stronger. Nevertheless, the separation from aqueous solution was trouble [10].

For overcoming this issue, the GO-based composites for adsorption have recently attracted considerable attention. Yang et al. [11] first reported the adsorption capacities of pristine natural zeolite, GO-grafted zeolite

* Corresponding author.

and benzene carboxylic acid derivatized graphene oxide nanosheets/natural zeolites for rhodamine B from water, and the maximums approached 50.25, 55.56 and 67.56 mg/g, respectively. Shao et al. [12] found that the maximum adsorption capacity of PANI/GO for U (VI) from aqueous solution attained 1,960 mg/g at pH = 5.0. Zhou et al. [13] found that the maximum adsorption capacity for volatile organic compounds onto ZIF-8/GO composites (with 15 wt% of GO) approached 240 mg/g [13]. Alternatively, we also intensively studied the adsorption capacities of the GO/beta composite containing 10 wt% of GO and GO/silicalite-1 containing 6 wt% of GO composite for RB removal from aqueous solution, and the maximums reached 51.55 and 64.47 mg/g, respectively [14,15]. The different-type zeolites have the distinctive pore channel, which significantly affects the adsorption capacity for dyes. The pore diameter and specific surface of Y-type zeolites are much larger than those of beta and silicalite-1, suggesting that the composites incorporated GO nanosheets should have the different adsorption behavior.

In this work, we successfully prepared the graphene oxide/Y-type zeolite composites. The effects of adsorption condition on the adsorption capacity of the composites for the removal of RB from aqueous solutions were extensively investigated. Finally, the adsorption behavior was studied by Langmuir and Freundlich models.

2. Materials and methods

2.1. Preparation of GO and Y-type zeolite powder

GO aqueous solution (0.69 wt%) was prepared from natural graphite powder (flaky graphite, >99.9995%) by the Hummers' method [16]. The oxidation product was purified by rinsing with 10% HCl solution, followed by washing with distilled water, and finally filtered through 0.22 μm nylon filter paper. The as-obtained filter cake was re-dispersed in distilled water with mild sonication (setting at 150 W for 4 h), obtaining GO aqueous solution (theoretical calculation value of 0.69 wt%). Y-type zeolite (SiO_2/Al_2O_3 = 3.15) was prepared by hydrothermal-synthesis method [17].

2.2. Surface activation of Y-type zeolite powder

First, 0.1 mL 32 wt% of aqueous hydrochloric acid was dropwise added into 0.5 g of Y-type zeolite suspension, and successively stirred for 30 min. Then, the resulting suspension was centrifuged at 3,000 rpm for 5 min, followed by successive washing with deionized water at least three times. Finally, the resulting powder was denoted acid-treated Y-type zeolite powder.

2.3. Preparation of GO-grafted Y-type zeolite

A certain amount of GO aqueous solution above was added into the above acid-treated Y-type zeolite suspension (0.05 g/mL). Then, it was subjected in ultrasound for 10 s, stirred for 30 min and then placed in an oven at 110°C for 12 h. Finally, the samples were filtrated, and subsequently washed with deionized water. The residues were marked as GY-1 (with 1 wt% of GO), GY-2 (with 6 wt% of GO) and GY-3 (with 10 wt% of GO), respectively.

2.4. Characterizations

The XRD patterns were recorded by powder X-ray diffraction (Bruker AXS, Germany). The Raman spectra were examined by Raman spectrometer (Renishaw, Britain). The FTIR spectra were measured with a Cary 610/670 micro infrared spectrometer (Varian, USA). The UV–Vis spectra were collected on a Cary 5000 spectrophotometer (Varian, USA). The Raman spectra were recorded by Raman spectrometer (Renishaw, Britain). The surface morphology was observed by S-4800 II field emission scanning electron microscopy (Hitachi, Japan) and Tecnai 12 transmission electron microscope (Philips, Netherlands). The EDS analysis was recorded by XL-30 environmental scanning electron microscope. The XPS spectra were recorded by ESCALAB 250Xi X-ray photoelectron spectrometer (Thermo Scientific, USA). BET specific surface areas were determined by using Sorptomatic 1990 Thermo Finningen Instrument (Thermo, USA). The AFM images were performed at a tapping mode by carrying out on a Nanoscope (Digital Instruments, USA).

2.5. Adsorption experiments

In this work, RB as model molecule was used to examine the adsorption performance of GY composites. The adsorbents (0.01 g) were dispersed in RB aqueous solution (10 mL). After reaching the adsorption equilibrium, the adsorbents were filtered through a 0.45 μm membrane. The filtrate was analyzed by using a UV-Vis spectrophotometer at a wavelength of 354 nm. The RB concentrations were calculated from a calibration curve. During absorption, hydrochloric acid or sodium hydroxide were used to adapt the pH value of solutions. Each sample was tested at least three times under the same conditions. The average adsorption capacity was given as following:

The RB adsorption capacity q (mg/g) was calculated from Eq. (1):

$$q = \frac{(C_0 - C)V}{W} \tag{1}$$

where C_0 and C represent the initial and equilibrium concentration of RB (mg/L), respectively; V and W expresses the solution volume (L) and the mass of the adsorbent (g), respectively.

3. Results and discussion

As shown in the XRD patterns of GO, Y-type zeolite and GY composites (Fig. 1), GO appears a typical diffraction peak at 2θ = 9.8° due to the presence of containing oxygen groups in the basal plane of natural graphite [18]. The peaks located at 2θ=(6.2°, 15.6°, 18.7°, 20.4°, 23.7°, 27.1°, 31.5°) indicate that the as-prepared Y-type zeolite is of faujasite structure. Compared with Y-type zeolite, the peak intensity of GY composites at 2θ = 9.8° gradually increases with the increase of the GO content. This should be ascribed to the increase of GO content.

Fig. 2 displays the SEM images of GO, Y-type zeolite and GY composites. The self-produced GO has the typical morphology of graphene. As shown in Figs. 2(c)–(e),

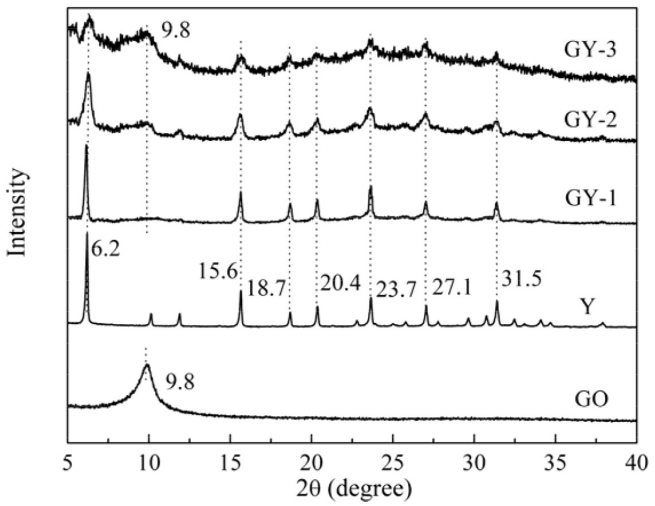

Fig. 1. XRD patterns of GO, Y-type zeolite and GY composites.

it is noteworthy that for the GY composites, the crystal surfaces of Y-type zeolite are covered by GO. More interestingly, it was also verified that those GO nanosheets coated on zeolite surface were good reservation despite subjecting under the repeated washing assisted with sonication in water. It suggests the existence of the strong interaction between Y-type zeolite and GO in composites. Accordingly, we deem that a chemical reaction between active groups of GO and Y-type zeolite surface was taken place, forming a covalent ester linkage [14,15]. In the EDX spectrum of GY-1 (Fig. 2(f)), a great deal of C element also emerges, suggesting the GO coated on the surface of Y-type zeolite.

Fig. 3 represents the FTIR spectra of GO nanosheets, Y-type zeolite and GY composites. The feature absorption peaks of GO are associated with 1,048 cm^{-1} (C–O–C); 1,221 cm^{-1} (C–O); 1,390 cm^{-1} (O–H); 1,624 cm^{-1} (C=C) and 1,731 cm^{-1} (C=O). There appears the O–H stretching vibration within 3,600–3,300 cm^{-1} corresponding to the hydroxyl and carboxyl groups of GO [19]. Regarding

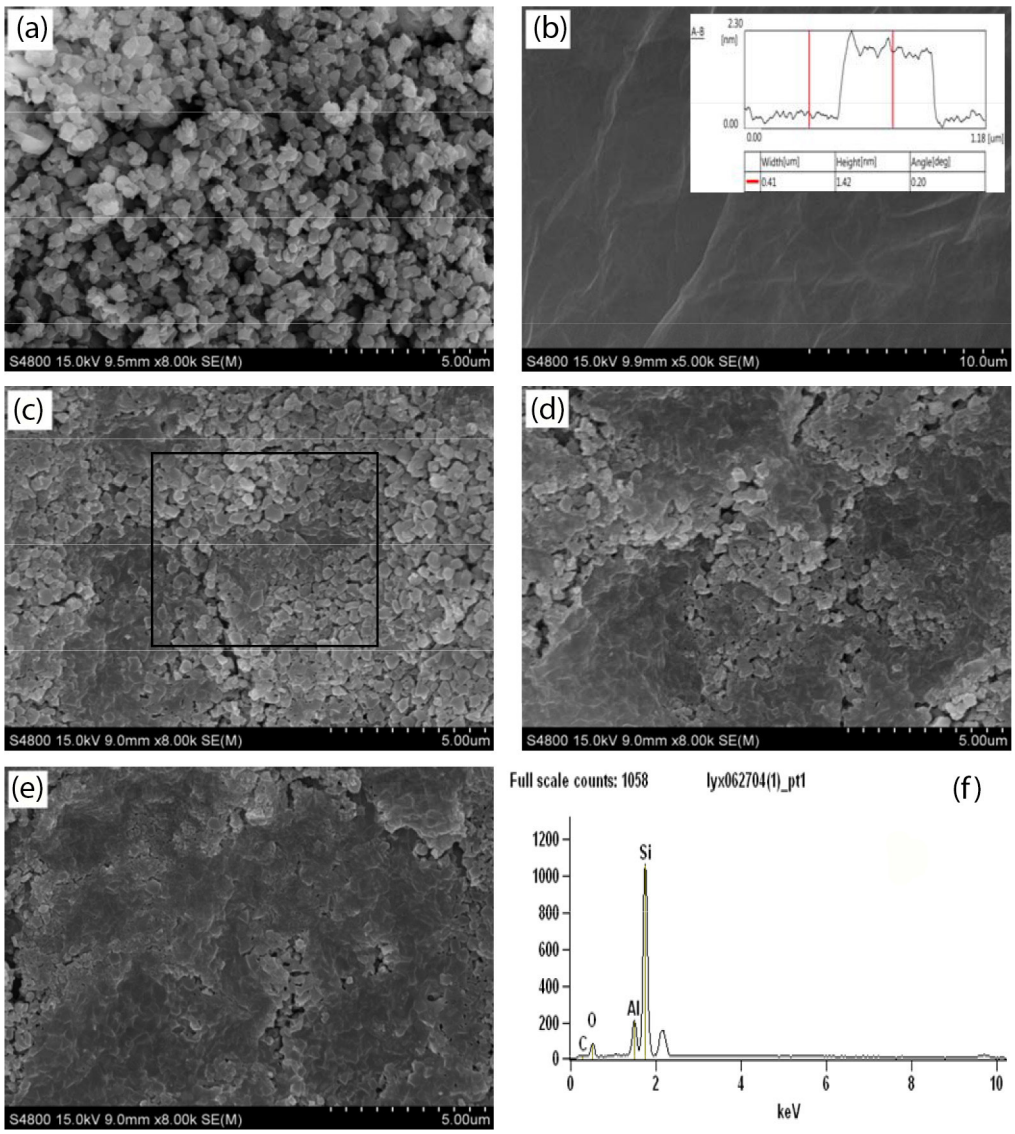

Fig. 2. SEM photos of (a) Y-type zeolite, (b) GO (inset: AFM), (c) GY-1, (d) GY-2, (e) GY-3 and (f) the EDX of GY-1.

Y-type zeolite, the O–H stretching vibrations appear at 3,620 and 3,429 cm^{-1}. The peaks at 510 and 1,040 cm^{-1} are corresponded to the six-membered ring and tetrahedron stretching vibration of Y-type zeolite. Definitely, there appear some additional bands at 1,331; 1,427 and 1,477 cm^{-1} for GY composites, which corresponds to the C–H stretching of GO, the asymmetric and symmetric stretching of carboxylate groups, respectively. The existence of the peak at 510 cm^{-1} for GY composites is assumed to non-destroy the structure of Y-type zeolite in grafting GO processing. This indicates that the functionalization of Y-type zeolite coated by GO nanosheets was successfully achieved.

The Raman spectra of GO nanosheets, Y-type zeolite and GY composites are shown in Fig. 4.the two characteristic peaks of GO lie at 1,354 and 1,597 cm^{-1} for all samples, being assumed to the typical D-band and G-band of GO, respectively. However, the intensity ratios of D/G increase obviously for the GY-1, GY-2, GY-3 (I_D/I_G = 0.8744, 0.9010, 0.9157) than that of GO (I_D/I_G = 0.7977), indicating the increase of the disordered carbon in the GY composites [20,21].

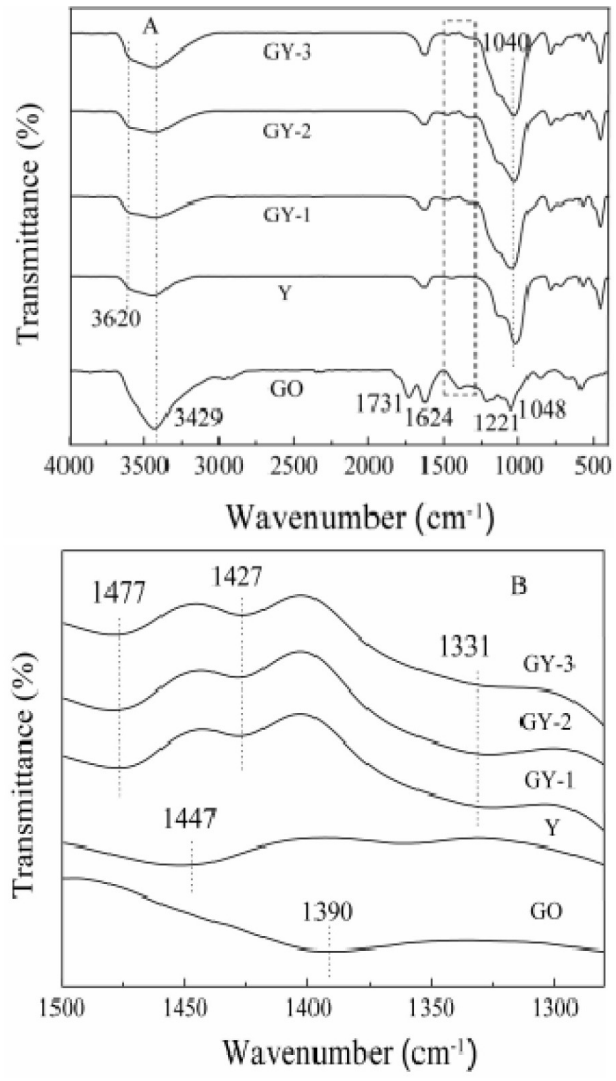

Fig. 3. FTIR spectra (a) and enlarged spectra (b) of skeletal vibration of GO, Y-type zeolite and GY composites.

Fig. 5 gives the UV-Vis absorption spectra of GO, Y-type zeolite and GY composites. As can be seen, GO has a strong absorbance peak (π-π* transition) at λ_{max} = 230 nm and a shoulder peak (*n*-π* transition) at 300 nm is associated with the carbonyl groups [19]. For composites, the absorption peaks around locate at 230 and 300 nm come from GO.

The survey and C 1s XPS spectra of GO, and GY composites are shown in Figs. 6(a) and (b). For GY composites, the percentages of carbon atoms are up to 11.48%, 15.13% and 18.87% for GY-1, GY-2 and GY-3, respectively. The C 1s spectrum of GO usually contains 284.8 eV of C–C/C=C, 286.8 eV of C–O, 288.0 eV of C=O and 289.0 eV of O–C=O. The oxidation degree of GO can be estimated by the peak intensity percentages of intact carbon (C–C/C=C) and oxygenated carbon atoms (C–O, C=O and O–C=O) [20]. In contrast to GO at 286.8 and 288.0 eV, the GY composites show the lower binding energy, indicating that GO should be hybridized with Y-type zeolite [22]. The decrease of the peak intensity percentages of the oxygenated carbon atoms

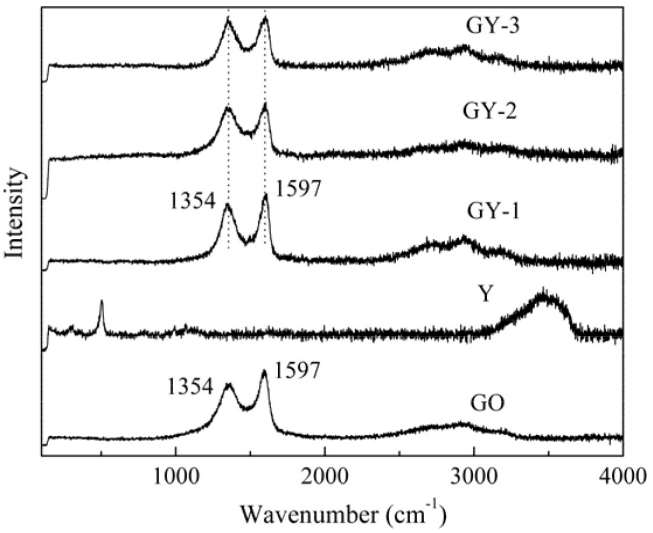

Fig. 4. Raman spectra of GO, Y-type zeolite and GY composites.

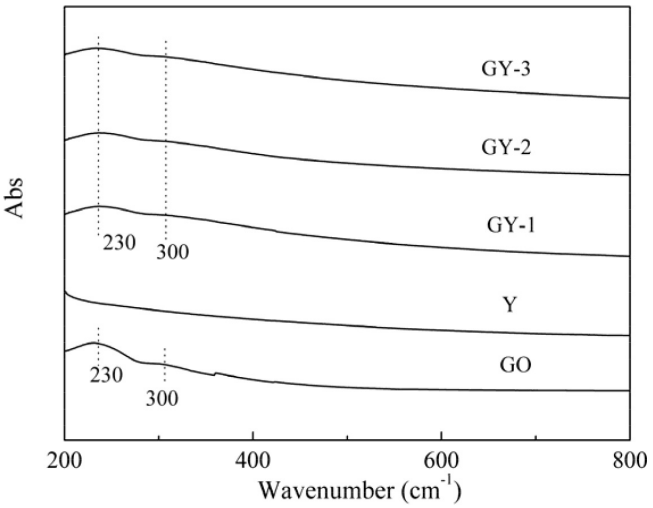

Fig. 5. UV-Vis spectra of GO, Y-type zeolite and GY composites.

suggests that between Y-type zeolite and GO nanosheets took place a bonded reaction. In spectrum of GY-3, there appears O–C=O (289.0 eV) because of enough high concentration of GO nanosheets on the Y-type zeolite surface [23].

Fig. 7 shows the N_2 adsorption–desorption and pore size distributions of Y-type zeolite and GY composites. As can be seen, the Y-type zeolite exhibits an adsorption mode of type I. However, the GY composites show an adsorption mode of type III. The isotherms of GY composites only show a hysteresis loop at high relative pressure, indicating the existence of mesopores. In addition, as summarized in Table 1, the surface area of the GY composites lessens with the increase of GO content. This is likely to be attributed to the increase of non-porous GO blocking the pore channels of Y-type zeolite [15]. The mesopore diameters of GY-1, GY-2 and GY-3 approach approximately 2.9, 3.0 and 3.0 nm, respectively. These mesopores should be formed from GO.

3.1. Adsorption of RB onto GY composites

Fig. 8 shows the adsorption capacities of Y-type zeolite and GY composites for RB depending on adsorption time. Obviously, the adsorption of RB onto these samples is rapid,

Table 1
BET properties of adsorbents

Samples	S_{BET}[a], m^2/g	S_{micro}[b], m^2/g	S_{meso}, m^2/g	V_{total}, cm^3/g	V_{micro}[c], cm^3/g	V_{meso}, cm^3/g
Y	428	366	62	0.281	0.214	0.067
GY-1	323	254	69	0.160	0.126	0.054
GY-2	252	190	62	0.104	0.105	0.039
GY-3	101	68	33	0.032	0.033	0.029

[a]BET method.
[b]t-plot method.
[c]DFT method.

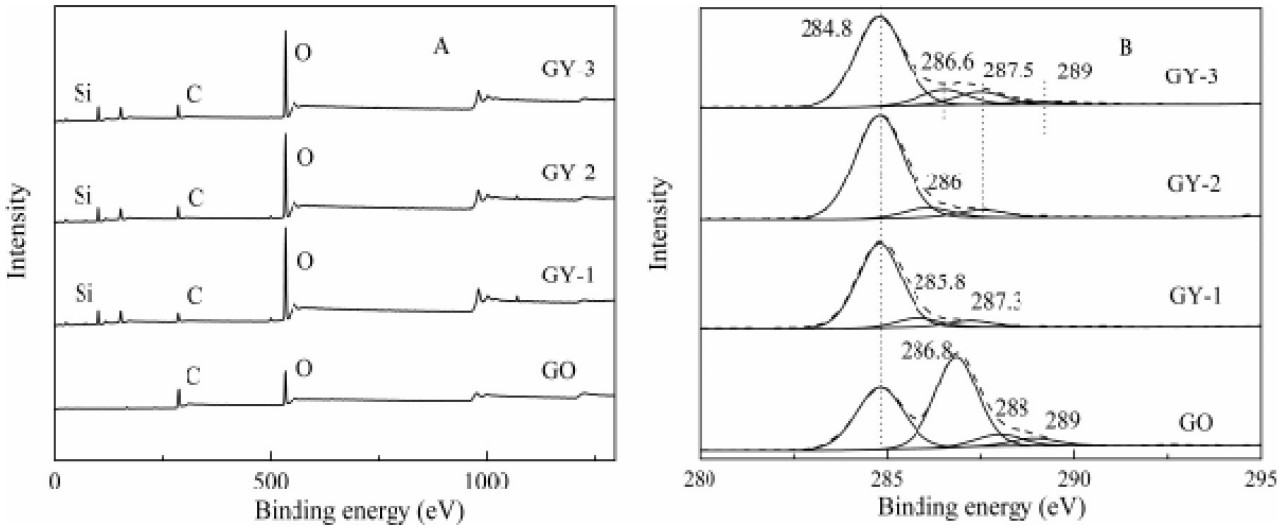

Fig. 6. Survey (a) and C 1s XPS spectra (b) of GO, Y-type zeolite and GY composites.

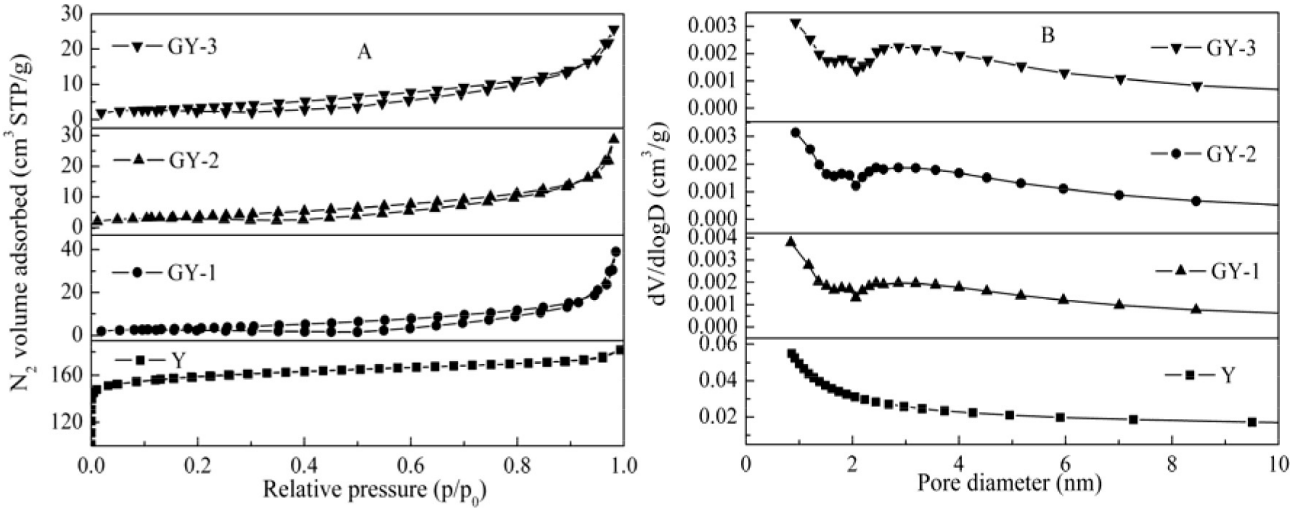

Fig. 7. N_2 adsorption–desorption isotherms (a) and pore size distributions (b) of Y-type zeolite and GY composites.

and reaches the equilibrium within 60 min. However, the equilibrium adsorption capacities of the GY composites are up to 4.53, 6.73 and 8.23 mg/g corresponding to GY-1, GY-2 and GY-3, respectively.

Fig. 9 shows adsorption of RB onto Y-type zeolite and GY composites depending on adsorption temperature. The adsorption capacity of these samples slightly rises with increasing the adsorption temperature, reflecting the endothermic process in the adsorption [2].

Fig. 10 shows the adsorption capacities of GY-1, GY-2 and GY-3 in range of pH = 3–9. The maximum adsorption capacity of Y-type zeolite approaches 4.40 mg/g at pH = 3, at which RB is thoroughly protonated [24,25]. After the surface functionalization, the adsorption capacities of GY-1, GY-2 and GY-3 at pH = 3 are up to 6.56, 9.83 and 11.57 mg/g, respectively. The indispensable electrostatic interactions between the GY and RB are conductive to the increase of adsorption capacity [10]. The potential hydrophobic and hydrogen bonding interactions of GO and RB can facilitate the adsorption [24].

Fig. 11 shows the adsorption of RB onto Y zeolite and GY composites in the RB initial concentration of 15–85 mg/L. To starting, the adsorption capacities of Y-type zeolite and GY initially rise swiftly and afterwards keep a slow increasing with the increase of RB concentration. The higher concentration is a strong driving force for mass transfer and subsequent surface adsorption on the adsorbents [26].

As shown in Fig. 12, the adsorption capacities of Y-type zeolite, GY-1, GY-2 and GY-3, respectively, attain 85.6%, 84.5%, 83.6% and 83.2% of fresh samples, even through the repeated adsorption–desorption operation was implemented three times. It suggests that the GY composites have a good recycling reusing performance. We deem that the loss of GO from the surface of zeolite results in the slight decrease.

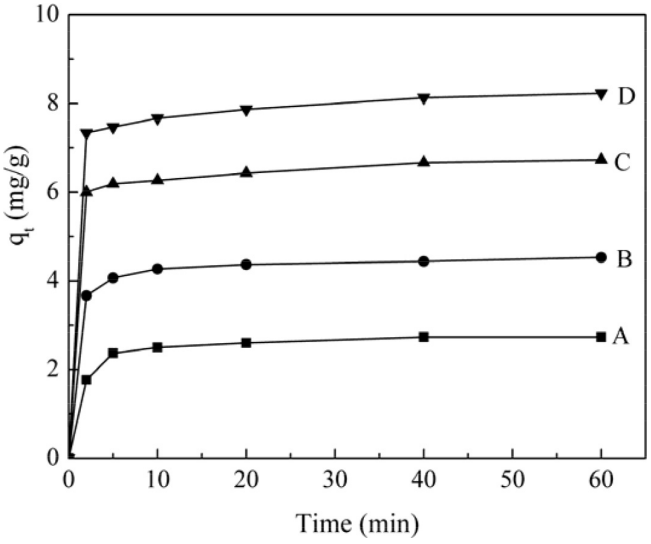

Fig. 8. Dependence of time on the adsorption of RB onto (a) Y-type zeolite, (b) GY-1, (c) GY-2 and (d) GY-3.

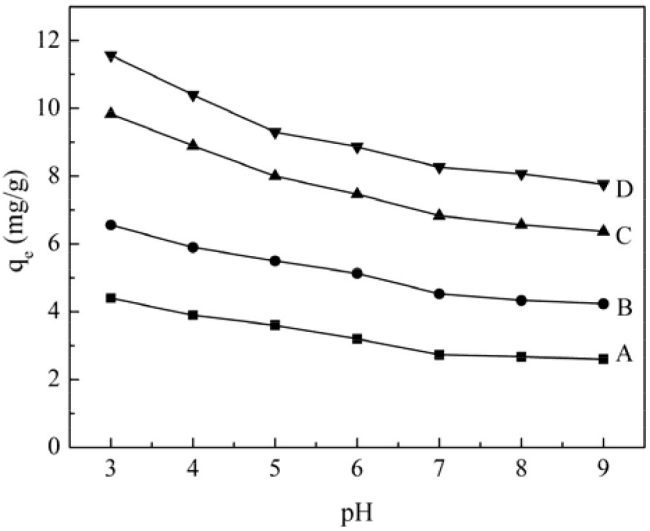

Fig. 10. Dependence of pH on the adsorption of RB onto (a) Y-type zeolite, (b) GY-1, (c) GY-2 and (d) GY-3.

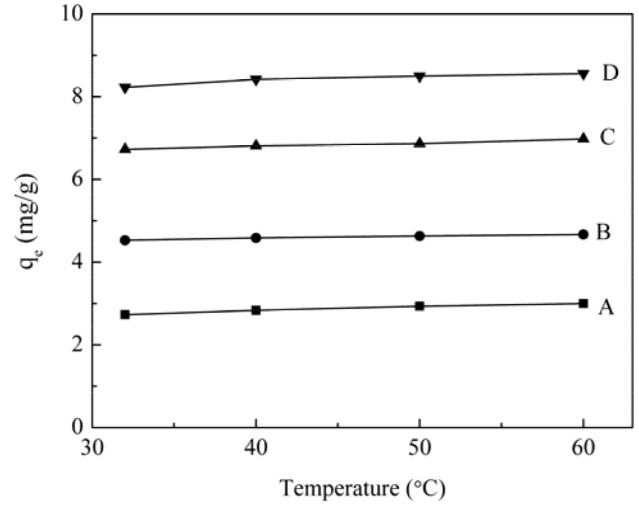

Fig. 9. Dependence of temperature on the adsorption of RB onto (a) Y, (b) GY-1, (c) GY-2 and (d) GY-3.

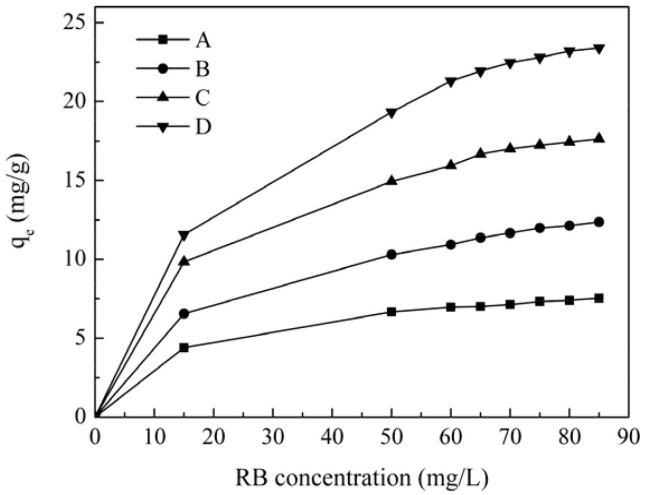

Fig. 11. Effect of the initial concentration on the adsorption of RB onto (a) Y-type zeolite, (b) GY-1, (c) GY-2 and (d) GY-3.

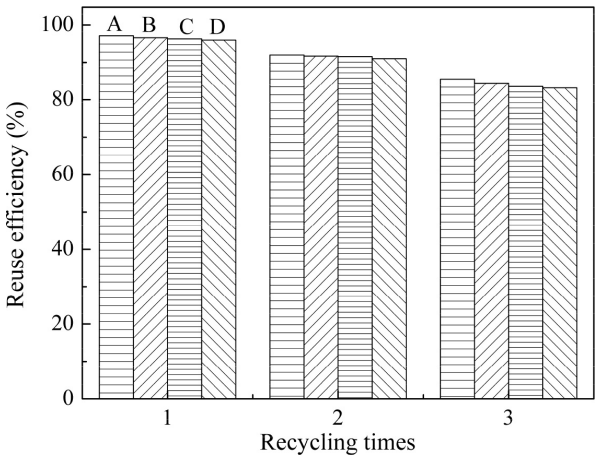

Fig. 12. Recycling performance of (a) Y-type zeolite, (b) GY-1, (c) GY-2 and (d) GY-3.

3.2. Adsorption isotherms

The linear form of Langmuir isotherm equation is expressed below:

$$\frac{C_e}{q_e} = \frac{C_e}{q_m} + \frac{1}{q_m b} \tag{2}$$

where q_e is the amount of MB adsorbed (mg/g), C_e is the equilibrium concentration (mg/L), q_m is maximum adsorption capacity (mg/g), b is a constant related to the energy of adsorption (L/mg). The values of q_m and b are calculated from the slope and intercept of the plot C_e/q_e vs. C_e.

The linear form of Freundlich isotherm equation is expressed as follows:

$$\log q_e = \log K_f + \frac{1}{n}\log C_e \tag{3}$$

where K_f (L/mg) and n are Freundlich constants, respectively, related to adsorption capacity and intensity of the adsorbent. Plotting log q_e against log C_e gives a straight line with intercept and slope equal to log K_f and 1/n.

Fig. 13 shows the Langmuir and Freundlich isotherms of Y-type zeolite and GY composites. The calculated data are listed in Table 2. The regression coefficients (R^2) of both Langmuir and Freundlich models are higher than 0.95, indicating good fitting to the experimental data. However, the Langmuir model (R^2 = 0.999, 0.992, 0.990, 0.993) has a better fitting than the Freundlich model (R^2 = 0.995, 0.980, 0.986, 0.985). This indicates that the Langmuir isothermal adsorption model is more suitable for describing the adsorption experiment data than the Freundlich model. The maximum adsorption capacities of Y-type zeolite, GY-1, GY-2 and GY-3 are 9.50, 14.83, 31.78 and 39.64 mg/g. The GY composites have the lower adsorption efficiency for RB than the result reported by Zhou et al. [10], which is ascribed to the different zeolite type. The possible adsorption mechanism is also proposed that the synergistic effects of the hydrogen bonding and the π–π electron stacking interactions between the adsorbent and adsorbate both contributed to the adsorption [27,28].

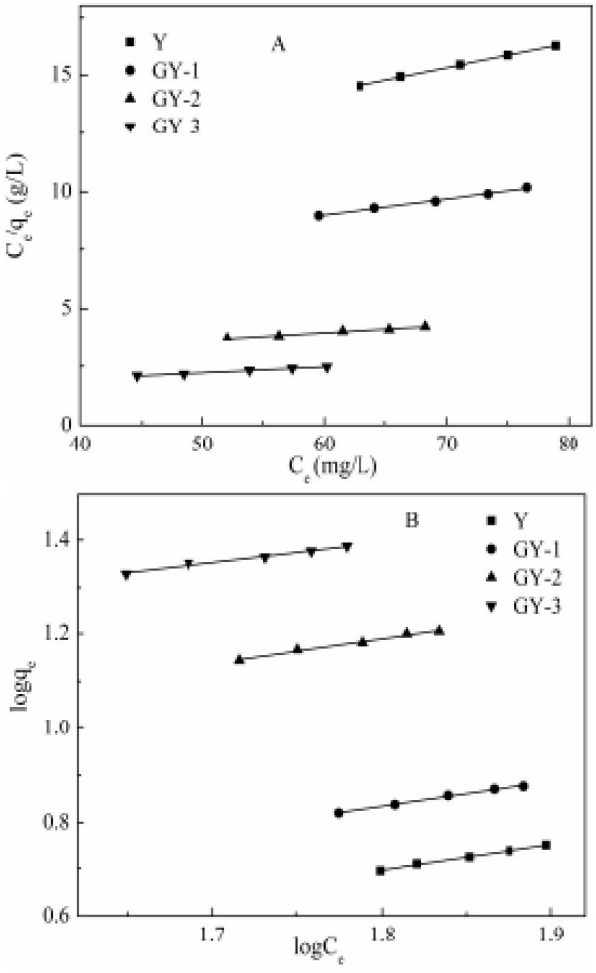

Fig. 13. Langmuir (a) and Freundlich (b) adsorption isotherm model fitting to experimental data.

Table 2
Langmuir and Freundlich isotherm model parameters for RB onto Y-type zeolite and GY

Sample	Langmuir model			Freundlich model		
	b (L/mg)	q_{max} (mg/g)	R^2	b (L/mg)	q_{max} (mg/g)	R^2
Y	0.0132	9.50	0.999	0.0132	9.50	0.999
GY-1	0.0136	14.83	0.992	0.0136	14.83	0.992
GY-2	0.0151	31.78	0.990	0.0151	31.78	0.990
GY-3	0.0264	39.64	0.993	0.0264	39.64	0.993

4. Conclusions

In summary, the novel graphene oxide/Y-type zeolite composites were prepared. The characterizations corroborated the binding existence between GO and Y-type zeolite. The GY composite material had a better adsorption capacity for RB dye than Y-type zeolite. The adsorption capacities for RB were up to 9.50 mg/g of Y-type, 14.83 mg/g of GY-1, 31.78 mg/g of GY-2, 39.64 mg/g of GY-3. The adsorption composites have a promising prospect in resolving dye wastewater.

Acknowledgment

This work was supported by the Talent Introduction Fund of Yangzhou University (2012), Key Research Project-Industry Foresight and General Key Technology of Yangzhou (YZ2015020), Innovative Talent Program of Green Yang Golden Phoenix (YZLYJFJH2015CX073), Yangzhou Social Development Project (YZ2016072), Jiangsu Province Six Talent Peaks Project (2014-XCL-013), Jiangsu Province Science and Technology Support Project (BE2014613) and Jiangsu Industrial-academic-research Prospective Joint Project (BY2016069-02). The data of this paper originated from the Test Center of Yangzhou University.

References

[1] X. Zhao, W. Wang, Y.J. Zhang, S. Wu, F. Li, J.P. Liu, Synthesis and characterization of gadolinium doped cobalt ferrite nanoparticles with enhanced adsorption capability for Congo Red, Chem. Eng. J., 250 (2014) 164–174.
[2] X.F. Wu, W. Wang, F. Li, S. Khaimanov, N. Tsidaevac, M. Lahoubi, PEG-assisted hydrothermal synthesis of $CoFe_2O_4$ nanoparticles with enhanced selective adsorption properties for different dyes, Appl. Surf. Sci., 389 (2016) 1003–1011.
[3] X.F. Wu, W. Wang, N.N. Song, X.J. Yang, S. Khaimanov, N. Tsidaeva, From nanosphere to nanorod: tuning morphology, structure and performance of cobalt ferrites via Pr^{3+} doping, Chem. Eng. J., 306 (2016) 382–392.
[4] B. Xu, C. Sievers, S.B. Hong, R. Prins, J.A.V. Bokhoven, Catalytic activity of Bronsted acid sites in zeolites: intrinsic activity, rate-limiting step, and influence of the local structure of the acid sites, J. Catal., 244 (2006) 163–168.
[5] C. Martínez, D. Verboekend, J. Pérezramírez, A. Corma, Stabilized hierarchical USY zeolite catalysts for simultaneous increase in diesel and LPG olefinicity during catalytic cracking, Catal. Sci. Technol., 3 (2012) 972–981.
[6] F. Sannino, S. Ruocco, A. Marocco, S. Esposito, M. Pansini, Cyclic process of simazine removal from waters by adsorption on zeolite H-Y and its regeneration by thermal treatment, J. Hazard. Mater., 229–230 (2012) 354–360.
[7] P. Sui, X. Meng, Y. Wu, Y. Zhao, L. Song, Z. Sun, L. Duan, Adsorption and diffusion of benzene and thiophene over Y/MCM-41 composite zeolite, Sci. Adv. Mater., 5 (2013) 1132–1138.
[8] L. Tan, S. Wang, W. Du, T. Hu, Effect of water chemistries on adsorption of Cs(I) onto graphene oxide investigated by batch and modeling techniques, Chem. Eng. J., 292 (2016) 92–97.
[9] Y. Li, Q. Du, T. Liu, X. Peng, J. Wang, J. Sun, Y. Wang, S. Wu, Z. Wang, Y. Xia, L. Xia, Comparative study of methylene blue dye adsorption onto activated carbon, graphene oxide, and carbon nanotubes, Chem. Eng. Res. Des., 91 (2013) 361–368.
[10] L. Zhou, H. Deng, J. Wan, R. Zhang, Synthesis and adsorption of graphene-based iron oxide magnetic nanocomposites, Prog. Chem., 25 (2013) 145–155.
[11] Y. Yang, B.N. Murthy, J.G. Shapter, K.T. Constantopoulos, N.H. Voelcker, A.V. Ellis, Benzene carboxylic acid derivatized graphene oxide nanosheets on natural zeolites as effective adsorbents for cationic dye removal, J. Hazard. Mater., 260 (2013) 330–338.
[12] D. Shao, G. Hou, J. Li, T. Wen, X. Ren, X. Wang, PANI/GO as a super adsorbent for the selective adsorption of uranium(VI), Chem. Eng. J., 255 (2014) 604–612.
[13] Y. Zhou, L. Zhou, X. Zhang, Y. Chen, Preparation of zeolitic imidazolate framework-8/graphene oxide composites with enhanced VOCs adsorption capacity, Microporous Mesoporous Mater., 225 (2016) 488–493.
[14] Z.L. Cheng, Y.X. Li, Z. Liu, Novel adsorption materials based on graphene oxide/Beta zeolite nanocomposites and their adsorption performance for rhodamine B, J. Alloys Compd., 708 (2017) 255–263.
[15] Z.L. Cheng, Y.X. Li, Z. Liu, Fabrication of graphene oxide/silicalite-1 composites with hierarchical porous structure and investigation on their adsorption performance for rhodamine B, J. Ind. Eng. Chem., 25 (2017) 234–243.
[16] Z.J. Li, F. Chen, L.Y. Yuan, Y.L. Liu, Y.L. Zhao, Z.F. Chai, W.Q. Shi, Uranium(VI) adsorption on graphene oxide nanosheets from aqueous solutions, Chem. Eng. J., 210 (2012) 539–546.
[17] Z.L. Cheng, E.Q. Gao, H.L. Wan, Novel synthesis of FAU-type zeolite membrane with high performance, Chem. Commun., 15 (2004) 1718–1719.
[18] L. Zhang, Y. He, S. Feng, L. Zhang, Z. Jiao, Y. Zhan, Y. Wang, Preparation and tribological properties of novel boehmite/graphene oxide nano-hybrid, Ceram. Int., 42 (2016) 6178–6186.
[19] J. Chen, Y. Li, L. Huang, C. Li, G. Shi, High-yield preparation of graphene oxide from small graphite flakes via an improved Hummers method with a simple purification process, Carbon, 81 (2015) 826–834.
[20] Y. Lu, Novel blue light emitting graphene oxide nanosheets fabricated by surface functionalization, J. Mater. Chem.. 22 (2012) 2929–2934.
[21] Y. Wang, Y. Gong, Y. Tian, L. Wang, Covalent bulk functionalization of grapheme, Nat. Chem., 3 (2011) 279–286.
[22] Y. Jiang, P. Liu, Y. Liu, X. Liu, F. Li, L. Ni, Y. Yan, P. Huo, Construction of amorphous Ta_2O_5/g-C_3N_4 nanosheet hybrids with superior visible-light photo activities for organic dye degradation and mechanism insight, Sep. Purif. Technol., 170 (2016) 10–21.
[23] L. Singh, P. Rekha, S. Chand, Cu-impregnated zeolite Y as highly active and stable heterogeneous Fenton-like catalyst for degradation of Congo red dye, Sep. Purif. Technol., 170 (2016) 321–336.
[24] R. Zhang, M. Hummelgrd, G. Lv, H. Olin, Real time monitoring of the drug release of rhodamine B on graphene oxide, Carbon, 49 (2011) 1126–1132.
[25] S.L. Hi, S.Y. Yong, C.L. Wong, Removal of rhodamine B from aqueous solution by sorption on *Turbinaria conoides* (Phaeophyta), J. Appl. Phycol., 21 (2009) 625–631.
[26] M.A. Al-Ghouti, M.A M. Khraisheh, M.N.M. Ahmad, S. Allen, Adsorption behaviour of methylene blue onto Jordanian diatomite: a kinetic study, J. Hazard. Mater., 165 (2009) 589–598.
[27] Z.L. Wu, Q. Liu, X.Q. Chen, J.G. Yu, Preconcentration and analysis of Rhodamine B in water and red wine samples by using magnesium hydroxide/carbon nanotube composites as a solid-phase extractant, J. Sep. Sci., 38 (2015) 3404–3411.
[28] J.Y. Yang, X.Y. Jiang, F.P. Jiao, J.G. Yu, The oxygen-rich pentaerythritol modified multi-walled carbon nanotube as an efficient adsorbent for aqueous removal of alizarin yellow R and alizarin red S, Appl. Surf. Sci., 436 (2018) 198–206.